Modelling the waterjet cable trenching process on sand dunes

Warringa, S.; Van Rhee, C.; Miedema, S. A.; Lupea, C.; Visser, C.

Publication date
2019

Document Version
Final published version

Published in
Proceedings 22nd World Dredging Congress

Citation (APA)
Warringa, S., Van Rhee, C., Miedema, S. A., Lupea, C., & Visser, C. (2019). Modelling the waterjet cable trenching process on sand dunes. In *Proceedings 22nd World Dredging Congress: WODCON 2019* (pp. 1135-1152). Chinese Dredging Association (CHIDA).

水下沙丘上射流开挖缆槽过程模拟

MODELLING THE WATERJET CABLE TRENCHING PROCESS ON SAND DUNES

S. Warringa,[1] C. van Rhee,[2] S.A. Miedema,[3] C. Lupea[4] and C. Visser[5]

摘要

近期在北海南部安装了许多海上风力发电场。内、外用电缆都被掩埋起来以防止掉落物或拖曳物的破坏。在沙质土壤中，采用遥控履带车辆进行掩埋。两个装有水射流的刀型器具用于流化沙子，并产生水-沙混合物的回流。北海南部的海底地形变化很大，以沙波和巨浪为特征。这些海底特征会显著阻碍沟槽开挖过程。目前，无法准确估计沙堆对挖沟过程的影响。沟槽的形成过程分为两部分：一部分是水流对海床的侵蚀（侵蚀模型），另一部分是泥沙在回流中的沉降（沉降模型）。

侵蚀模型的建立基于这样一个假设：使沙子流动所需的特定能量等于用刀片切割沙子所需的特定能量。根据Miedema（2015年）一文，叶片被认为具有较小的叶片角度，并能在零米水深下运作。对于给定的喷射配置和沟槽尺寸，这会导致挖沟机速度受限。原位土、射流水量和挟带水流之间的体积平衡提供了反洗流速和浓度。最后两个被用作沉降模型的输入。

根据浅水方程，沉积模型将水流、泥沙输移、河床演变和沟槽宽度的演变联系起来。控制方程代表了水沙混合物的水平动量和质量守恒，以及泥沙的水平质量守恒。本文提出了一个一维有限体积数值模型，该模型在交错网格上求解。

弹性悬臂梁模型被用以确定缆线在沟槽中下沉时的形状。随后，缆线的下降深度由缆线与沟槽形状的交叉点确定。结合全尺寸现场数据，验证了流化、沉降和缆线组合模型。

关键词：缆线开挖；数值模拟；特定能量；侵蚀；沉积；分裂

[1]硕士研究生，离岸及疏浚工程，代尔夫特理工大学，Mekelweg 2, Delft, Netherlands，电话：+31 6152 109 35，Email: sjoerdwarringa@gmail.com

[2]疏浚工程全职教授，代尔夫特理工大学，Mekelweg 2, Delft, The Netherlands，电话：+31 15 2783973，Email: C.vanRhee@tudelft.nl

[3] 疏浚工程副教授，代尔夫特理工大学，Mekelweg 2, Delft, The Netherlands，电话：+3115 278 8359，Email: S.A.Miedema@tudelft.nl

[4]土木工程师，Tideway Offshore Solutions公司， Minervum 7442, 4817ZG, Breda, The Netherlands，电话：+31 76 520 4140，Email: Lupea.Cristina@deme-group.com

[5]工程经理，Tideway Offshore Solutions公司， Minervum 7442, 4817ZG, Breda, The Netherlands，电话：+31 76 513 7213

MODELLING THE WATERJET CABLE TRENCHING PROCESS ON SAND DUNES

S. Warringa,[1] C. van Rhee,[2] S.A. Miedema,[3] C. Lupea[4] and C. Visser[5]

ABSTRACT

Numerous offshore wind farms have been installed recently in the southern part of the North Sea. Their infield and export cables are buried for protection against dropped or dragged objects. In sandy soils, burial is carried out by remotely operated tracked vehicles. Two swords with waterjets are used to fluidize the sand and generate a backward flow of the water-sediment mixture. The southern part of the North Sea has a highly variable seabed topography characterized by sand waves and megaripples. These seabed features can hinder significantly the trenching process. At the moment it is not possible to make an accurate estimate of the influence of sand dunes on the trenching process. The trench formation process is split into two parts; a front section where the seabed is eroded by waterjets (erosion model) and a rear section where the sand grains are settling in a backward flow (sedimentation model).

The erosion model is made based on the assumption that the specific energy required to fluidise sand is equal to the specific energy required to cut sand with a blade. The blade is considered to have a small blade angle and to operate at zero meter waterdepth, following Miedema (2015). For a given jetting configuration and trench dimensions this results in a limiting trencher velocity. A volume balance between situ soil, waterjet flow and entrained flow gives the backwash flow rate and concentration. The last two are used as input for the sedimentation model.

The sedimentation model relates water flow, sediment transport, bed evolution and trench width evo- lution, based on the shallow water equations. The governing equations represent horizontal momentum and mass conservation of the water-sediment mixture and horizontal mass conservation of the sediment. A numerical one-dimensional finite volume model is proposed, which is solved on a staggered grid.

An elastic cantilever beam model is used to determine the cable shape as it sinks in the trench. Sub- sequently the depth of lowering of the cable is determined by the intersection of the cable and trench shape. The combined fluidization, sedimentation and cable model is validated against full scale field data.

Keywords: Cable trenching, Numerical modelling, Specific energy, Erosion, Sedimentation, Breaching

INTRODUCTION

Offshore cables are commonly buried for protection against dropped or dragged objects. In sandy soils, burial is carried out by remotely operated tracked vehicles, see figure 1a. Two swords with waterjets are located in between the tracks of the vehicle, on either side of the cable. Water is pumped through the swords to fluidize the sand and generate a backward flow of the water-sediment mixture, see figure 1b. The cable located on the seabed is lowered into the water-sediment mixture due to its own weight. Due to waves, tides and currents, sandy seabeds are often not flat, but can contain seabed features such as sand waves and megaripples. When burying a cable in these seabed features, the achieved depth of lowering shows an oscillating profile, with the maximum depth of lowering achieved at the peaks of these features and minimum at their troughs. Models to predict the

[1]MSc student, Offshore & Dredging Engineering, Delft University of Technology, Mekelweg 2, Delft, Netherlands, T: +31 6 152 109 35, Email: sjoerdwarringa@gmail.com

[2]Full Professor of Dredging Engineering, Delft University of Technology, Mekelweg 2, Delft, The Netherlands, T: +31 15 2783973, Email: C.vanRhee@tudelft.nl

[3]Associate Professor of Dredging Engineering, Delft University of Technology, Mekelweg 2, Delft, The Netherlands, T: +31 15 278 8359, Email: S.A.Miedema@tudelft.nl

[4]Geotechnical Engineer, Tideway Offshore Solutions, Minervum 7442, 4817ZG, Breda, The Netherlands, T: +31 76 520 4140, Email: Lupea.Cristina@deme-group.com

[5]Engineering Manager, Tideway Offshore Solutions, Minervum 7442, 4817ZG, Breda, The Netherlands, T: +31 76 513 7213, Email: Visser.Connie@deme-group.com

achieved depth of lowering are currently not able to account for the influence of seabed features, therefore an attempt has been made in modelling the effect of seabed features on the depth of lowering.

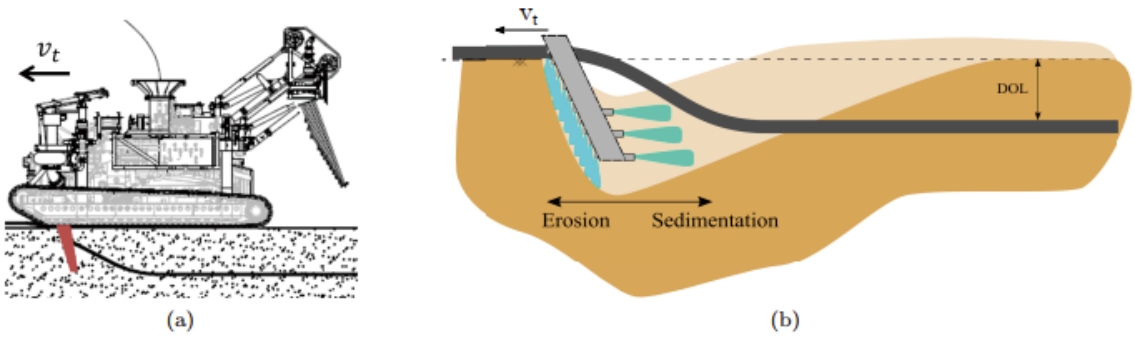

Figure 1. Typical waterjet trencher with the jet swords indicated in red (a), illustration of the erosion, sedimentation and cable component of the jet trenching model (b).

To make an accurate prediction of the depth of lowering of a cable, modelling is divided into three parts; a model for the erosion section, a model for the sedimentation section and a model for the cable deflection. The erosion model determines the maximum trencher velocity at which the seabed can still be eroded. Furthermore it provides flow input values for the sedimentation model. The sedimentation model determines the shape of the trench behind the vehicle. By iteratively calculating the cable shape in the cable deflection model, the point of intersection with the trench shape is determined. It is assumed that cable remains fixed in this point of intersection, hereby giving the achieved depth of lowering. See figure 2 and 7a for an illustration of the jet trenching model working principle.

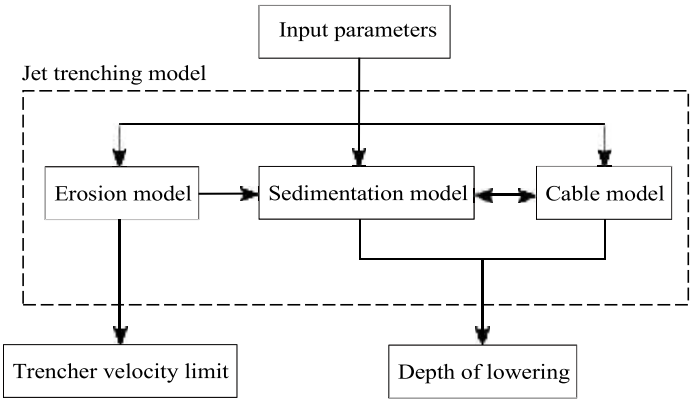

Figure 2. Schematisation of the interaction between erosion, sedimentation and cable model with corresponding outputs.

EROSION MODEL

At the front of the trench, sand is eroded by the water flow from the jet swords. It is assumed that the erosion process results in well-mixed backward flow of water and sediment. Via a volume balance the backward flow rate and sediment concentration is determined. Via a specific energy approach the maximum trencher velocity is determined at which the jets are still able to sufficiently erode the seabed. It is assumed that below this trencher velocity there are no problems to erode the seabed.

Limiting Trencher Velocity Using A Specifte Energy Approach

Miedema, 2015 derived a theory for the in-situ production of jets in a draghead. It is based on the assumption that the specific energy required to fluidise sand is equal to the specific energy required to cut sand with a blade, having a small blade angle and at zero meter waterdepth. The in-situ production Q_{situ} (sand plus pore water) of the jet trencher is given by equation 1, where d_{max} and b_0 are initial trench depth and width respectively and v_t is the trencher velocity. The in-situ production can also be defined by dividing jet power P_j by specific energy $E_{sp.}$

$$Q_{\text{situ}} = A_{trench} \cdot v_t = d_{max} \cdot b_0 \cdot v_t = \frac{P_j}{E_{SP}} \quad (1)$$

The specific energy is determined by assuming it to be equal to that of non-cavitating cutting, given by equation 2. Where ε is dilatency, km is mean permeability and ρ_w is seawater density. Horizontal force coefficient c_1 must be calibrated using experiments, Miedema (2015) suggests a value of 0.12. This value is based on calibration with experiments done by "*Combinatie Speurwerk Baggertechniek*", published in (Jong, 1988).

$$E_{sp} = c_1 \cdot \rho_w \cdot g \cdot h_i \cdot v_t \frac{\varepsilon}{k_m} \quad (2)$$

For cutting sand with a blade the parameter h_i is the layer thickness. Since the jet swords have numerous jets spaced vertically, this does not directly relate. A reasonable assumption is to consider the trench as a whole and therefore assume h_i to be equal to the trench depth d_{max}. The ratio of mean permeability to dilatancy can be approximated using the Kozeny Carman equation, resulting in the following relation.

$$\frac{k_m}{\varepsilon} \approx 10 \cdot k_0 \quad (3)$$

Total jet power P_j is given by the product of jet pressure and flow rate, where flow rate is determined by jet pressure p_j and nozzle diameter D_j. By combining the equations mentioned before, the maximum trench depth d_{max} is found as a function of soil parameters, jetting parameters and trencher speed v_t. Since the sword depth is an input, the maximum trencher velocity can be determined by the intersection of sword depth and maximum trench depth d_{max}.

$$d_{max} = \left[\frac{p_j \cdot n_j \sqrt{\frac{2p_j}{\rho_w}} \frac{\pi}{4} (\alpha_c \cdot D_j)^2 \cdot 10 \cdot k_0}{c_1 \cdot v_t^2 \cdot \rho_w \cdot g \cdot b_0} \right]^{1/2} \quad (4)$$

An example of this relation is given in figure 3 from which can be concluded that the trencher should not have any problem to fluidise the seabed up to a trencher velocity of approximately 600m/hr.

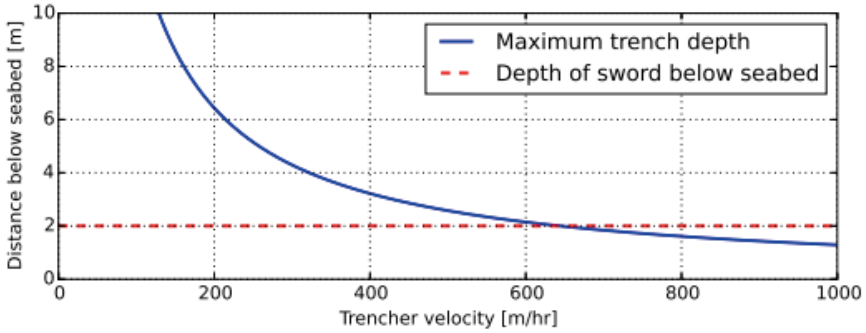

Figure 3. Maximum trench depth based on the speciftc energy approach (blue line) and depth of sword below the seabed (dashed red line). Plotted example is for a jet pressure of 8bar**, total number of forward nozzles** $n_j = 28$ **with a diameter of** D_j = 14mm **and a trench width of** b = 0.75m.

Volume Conservation

To determine the flow rate and concentration at the interface between the erosion and sedimentation section a volume conservation is applied. The flow rate and concentration are used as input for the sedimentation

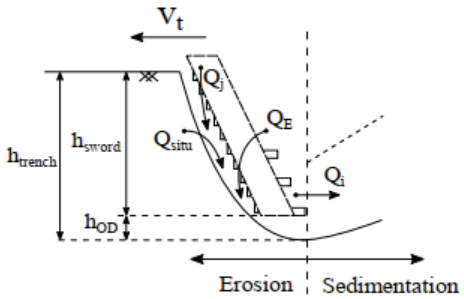

Figure 4. Flow idealization of the erosion section; volume balance of in-situ, jet and entrained flow rate.

model. The interface flow rate Q_i is simply determined by the sum of the in-situ soil flow rate Q_{situ}, waterjet flow rate Q_j and flow rate of clear seawater entrained in the flow Q_E , see equation 5 and figure 4.

$$Q_i = Q_j + Q_{situ} + Q_E = \left(Q_{j,fwd} + Q_{j,iwd} + Q_{j,bw}\right) + Q_{situ} + Q_E \quad (5)$$

In which Q_j is the total jet flow rate and thus the sum of forward, inward and backwash jets, see equation 5. Jet flow rates are calculated by using the Bernoulli theory, see equation 6 for the flow rate of a single nozzle, ignoring internal pressure losses.

$$Q_{j,single} = \sqrt{\frac{2 \cdot \Delta p_j}{\rho_w}} \frac{\pi}{4} (\alpha_c \cdot D_j)^2 \quad (6)$$

In-Situ Flow Rate

In-situ flow rate Q_{situ} is defined as the maximum trench cross sectional area times the trencher velocity. Maximum trench depth is given by the depth of the swords below the seabed plus a certain overdepth h_{OD}. The overdepth is calculated as a fraction (α_{OD}) of maximum trench depth dmax, calculated by the specific energy approach. By using this method, the overdepth is dependent on trencher velocity, jetting power and seabed permeability. After calibration a reasonable assumption was found to be $\alpha_{OD} = 0.03$.

$$h_{OD} = \alpha_{OD} \cdot d_{max} \quad (7)$$

The initial trench width b_0 is assumed to be approximately the same as the sword separation distance (outside to outside), plus a small margin. The in-situ flow rate is now given by equation 8.

$$Q_{situ} = v_t \cdot A_{trench}$$
$$= v_t \cdot (h_{sword} + h_{OD}) \cdot b_0 \quad (8)$$

Entrainment Of Ambient Water

A certain amount of ambient water will entrain the flow before reaching the transition between erosion and sedimentation. Due to the complex flow pattern and lack of experimental data it is difficult to say which mechanisms are taking place. Therefore to estimate the entrainment flow rate some simplifications and assumptions have to be made.

- Flow entrainment is based on entrainment calculations for free non-cavitating jets.
- Water is only entrained at the backside of the jet, see figure 5a. On the front side of the jets in-situ soil is loosened, which is not considered as entrainment but is included in the volume conservation.

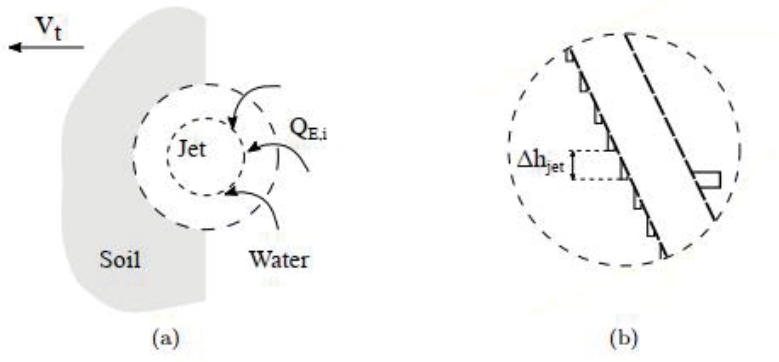

Figure 5. Cross-section of jet flow where water is only entrained at the backside (a), an illustration of vertical jet spacing (b).

- Water is entrained in an individual jet over a distance equal to the vertical spacing between individual jets, Δh_{jet} (figure 5).
- Water is only entrained in the forward jets located on the top half of the jet swords, the inward and backwash jets are neglected.

The total entrained flow rate is determined by the summation of entrainment per individual jet. For a single jet sword the number of forward jets at the top half of the sword is given by N . Consequently the total entrained flow rate is given by equation 9.

$$Q_E = 2 \cdot \sum_{i=1}^{N} Q_{E,i} \quad (9)$$

Of which the entrainment for a single jet, for a distance from zero to Δ_{hjet} is given by equation 10.

$$Q_{E,i} = \alpha_E \cdot \pi \int_0^{\Delta_{hjet}} r_u(s) u_u(s) ds \quad (10)$$

In a free turbulent jet two regions can be defined; a region of flow development and a region of fully developed flow. For the flow development region the entrainment coefficient is half of the fully developed flow region entrainment coefficient. For a free non-cavitating jet a reasonable assumption is $\alpha_E = 0.085$ in the fully developed flow region and a value of k = 77 for the empirical constant k, as given in Nobel (2013). Also the development of the uniform flow velocity u_u and jet radius r_u is different in the flow development region and region of fully developed flow. Analytical expressions are derived in Lee and Chu (2003) and are given by equation 11, 12, 13 and 14.

For $S < S_{dr}$: $u_u(s) = u_o \frac{D_j\sqrt{k/2}}{s+D_j\sqrt{k/2}}$ (11)

$$r_u(s) = \frac{1}{\sqrt{2k}} s + \frac{1}{2} D_j \quad (12)$$

For $S \geqslant S_{dr}$: $u_u(s) = \frac{1}{2}\sqrt{\frac{k}{2}} u_0 \frac{D_j}{s}$ (13)

$$r_u(s) = \sqrt{\frac{2}{k}} s \quad (14)$$

The position S_{dr} where the transition from flow development region to developed flow region is, can be can be determined by $S_{dr} = \sqrt{k/2} \approx 6.2 D_j$. Now equations 10 to 14 can be combined and simplified resulting in equation 15. The first term gives the entrainment in the flow development zone, and the second term is the entrainment in the developed flow region, up to a distance Δh_{jet}.

$$Q_{E,i} = \pi \frac{\alpha_E}{2} \int_0^{6.2 D_j} \left(\frac{1}{\sqrt{2k}} s + \frac{1}{2} D_j \right) \left(u_0 \frac{D_j\sqrt{k/2}}{s+D_j\sqrt{k/2}} \right) ds + \frac{\pi}{2} \alpha_E \cdot u_0 \cdot D_j \left(\Delta h_{jet} - 6.2 \cdot D_j \right) \quad (15)$$

Output To Sedimentation Model

The flow rate and concentration are determined by equation 16 and 17. Where the entrained flow rate is corrected by a factor $(1-c_0)$. This correction results from the assumption that the entrained water is not completely sediment-free but has a concentration equal to the output concentration. Equation 16 is therefore implicit and must be solved iterative.

$$c_0 = \frac{(1-n_0) \cdot Q_{situ}}{Q_{situ} + Q_j + Q_E \cdot (1-C_0)} \quad (16)$$

$$Q_0 = Q_{situ} + Q_j + Q_E \cdot (1 - C_0) \quad (17)$$

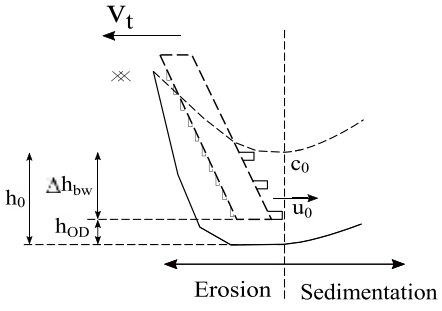

Figure 6. Output values to the sedimentation model in case of a supercritical flow (u_0 and h_0) or subcritical flow (Q_0).

SEDIMENTATION MODEL

The sedimentation model describes the backward flow containing water and suspended sediment. Input variables used from the erosion model are initial trench dimensions, flow rate and sediment concentration. Included in the sedimentation model is breaching of trench sidewalls, entrainment of ambient water and erosion/sedimentation of the trench bottom. Breaching is included via the active wall velocity, v_{wall} in figure 7b. The sidewalls are assumed to be and remain vertical. Furthermore it is assumed that the material coming from the side walls is mixed instantaneous in the backward flow, hereby conserving the rectangular trench shape. All main parameters are illustrated in figure 7a and 7b. Notable are the constant concentration c and velocity u over the vertical axis, and the distinction between initial seabed porosity n_o and re-settled seabed porosity n_s.

Shallow Water Equations For Flow In A Rectangular Channel With Variable Cross-Section

To model the flow of water and sediment behind the trencher, the so-called *Shallow Water Equations (SWE)* are used, first proposed by Saint Venant (1871) and therefore also sometimes referred to as the *Saint-Venant equations*. It is assumed that the flow is one-dimensional, hereby reducing the system of equations to only three.

- Continuity of the total fluid volume (water plus sediment), see equation 18.

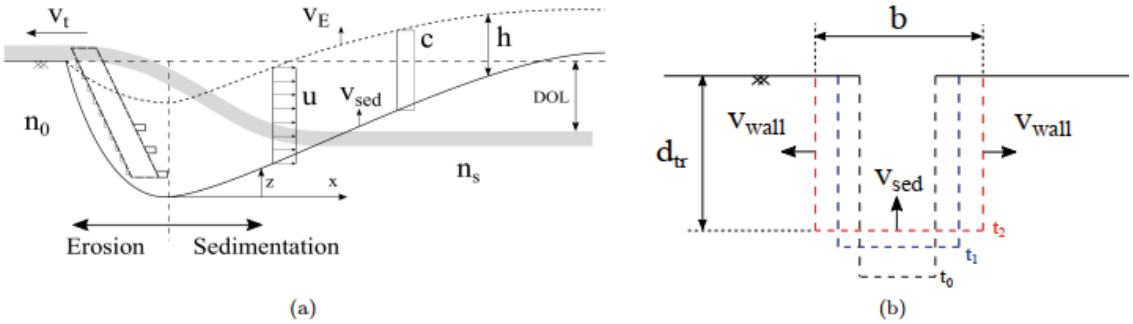

Figure 7. Trench side view (a) and cross-section (b), showing all main parameters used in the sedimentation model. ($t_0 < t_1 < t_2$)

- Continuity of sediment volume, see equation 19.
- Conservation of momentum, see equation 20.

Furthermore it is assumed that all quantities are uniform over the cross-section and vertical velocities are neglected. To simplify the solving of the momentum equation, it is rewritten so that the concentration is not present in the time derivative anymore, similar to (He et al., 2014) and (Cao et al., 2004).

$$\frac{\partial(hb)}{\partial t} + \frac{\partial(hub)}{\partial x} = (v_E - v_{sed})b + 2 \cdot v_{wall} \cdot d_{tr} \tag{18}$$

$$\frac{\partial(hbc)}{\partial t} + \frac{\partial(hbuc)}{\partial x} = -v_{sed}(1 - n_s)b + 2 \cdot v_{wall}(1 - n_0)d_{tr} \tag{19}$$

$$\frac{\partial(hbu)}{\partial t} + \frac{\partial(hbu^2)}{\partial x} + \frac{1}{2}g\frac{\partial(bh^2)}{\partial x} = S_{bed} + S_f + S_{sed} + S_c + S_\omega \tag{20}$$

Where h is flow height, b is trench width, u is mean flow velocity and c is sediment concentration. Furthermore v_E is the entrainment velocity, S_{sed} the sedimentation velocity (i.e. vertical velocity of the bed), v_{wall} the active wall velocity due to breaching, n_0 and ns are the porosity of the initial and re-settled seabed respectively and d_{tr} the trench depth. The source terms on the right hand side in the momentum equation (eq. 20) are given separately in equation 21 to 25 for improved readability. These source terms S_{bed}, S_f , S_{sed}, Sc and S_ω account for the bed gradient, bed friction, sediment exchange, concentration gradient and divergence of the trench width respectively. The source term S_ω is not present in the classical form of the shallow water equations, where the width is considered

constant. However, it arises in the derivation of the shallow water equations in a channel of varying width, see for example (Robert and Wilson, 2011) or (Siviglia et al., 2008).

$$S_{bed} = -\mathrm{g} \cdot \mathrm{h} \cdot \mathrm{b}(\frac{\partial_z}{\partial x} - \tan(\theta)) \tag{21}$$

$$S_f = -u_*^2(2 \cdot d_{tr} + b) \tag{22}$$

$$S_{sed} = v_{sed} \cdot u \cdot \mathrm{b} \frac{(\rho_{settled} - \rho)}{\rho} \tag{23}$$

$$S_c = -\frac{1}{2} g \cdot b \cdot h^2 \frac{(\rho_s - \rho_w)}{\rho} \frac{\partial_c}{\partial_x} \tag{24}$$

$$S_w = \frac{1}{2} g \cdot h^2 \frac{\partial_b}{\partial_x} \tag{25}$$

The system of equations is completed with the description of the evolution of trench width b in time (equation26) and evolution of bed evolution *z* in time (equation 27).

$$\frac{\partial_b}{\partial_t} = 2 \cdot v_{wall} \tag{26}$$

$$\frac{\partial_z}{\partial_t} = v_{sed} \tag{27}$$

Lastly, the definition of mixture density ρ is given by equation 28 and the density of the seabed after it has re-settled again by equation 29.

$$\rho = \mathrm{c} \cdot \rho_s + (1 - c) \cdot \rho_\omega \tag{28}$$

$$\rho_{settled} = \mathrm{n}_s \cdot \rho_\omega + (1 - n_s) \cdot \rho_s \tag{29}$$

One-Dimensional Finite Volume Scheme On A Staggered Grid

The equations are solved on a one-dimensional staggered grid, using a finite volume scheme. In the staggered grid the flow height h and concentration c are discretised at the center of each cell. The flow velocity *u* is discretised at the interfaces between the cells. Corresponding to the descretised variables, the control volume for continuity equations is centered around the *h*, *c* and *u* variables, whereas the control volume of the momentum equation is centered around velocity u and is thus staggered with respect to the continuity control volume, see figure 8. The change in width is only a function of the wall velocity (eq. 26), which is a known constant. Therefore the width is known at every grid point and every time step and thus no approximations are required. The continuity equation for the total volume and the continuity equation for the sediment volume are discretised explicit in time and upwind for the fluxes, see equations 30 and 31. The variables that are not defined on the grid are denoted with a hat and determined via an upwind approximation. Time steps are indexed by superscript n and space steps by subscript *i*.

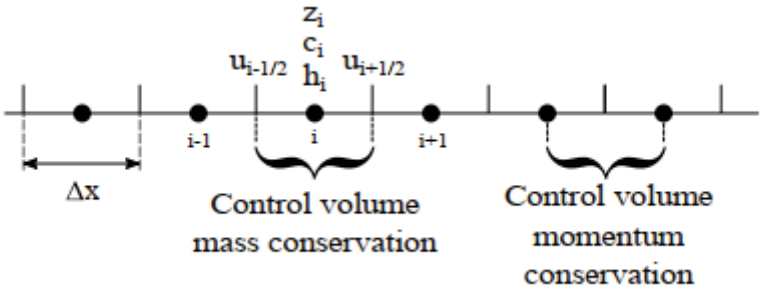

Figure 8. Deftnition of the discrete variables on the staggered grid, with corresponding control volumes.

$$\frac{h_i^{n+1}b_i^{n+1}-h_i^n b_i^n}{\Delta t}+\frac{\hat{h}_{i+1/2}^n u_{i+1/2}^n b_{i+1/2}^n-\hat{h}_{i-1/2}^n u_{i-1/2}^n b_{i-1/2}^n}{\Delta x}$$

$$=[(v_E)_i^n-(v_{sed})_i^n]b_i^n+2v_{wall}(d_{tr})_i^n \tag{30}$$

$$\frac{h_i^{n+1}b_i^{n+1}c_i^{n+1}-h_i^n b_i^n c_i^n}{\Delta t}+\frac{\hat{h}_{i+1/2}^n b_{i+1/2}^n u_{i+1/2}^n \hat{c}_{i+1/2}^n-\hat{h}_{i-1/2}^n b_{i-1/2}^n u_{i-1/2}^n \hat{c}_{i-1/2}^n}{\Delta x}$$

$$=-(v_{sed})_i^n(1-n_s)b_i^n+2v_{wall}(1-n_0)(d_{tr})_i^n \tag{31}$$

The momentum equation is discretised on a staggered grid, see equation 32 for the discretised equation.

$$\frac{\hat{h}_{i+1/2}^{n+1}b_{i+1/2}^{n+1}u_{i+1/2}^{n+1}-\hat{h}_{i+1/2}^n b_{i+1/2}^n u_{i+1/2}^n}{\Delta t}+\frac{h_{i+1}^n b_{i+1}^n(\hat{u}_{i+1}^n)^2-h_i^n b_i^n(\hat{u}_i^n)^2}{\Delta x}+\frac{1}{2}g\frac{(h_{i+1}^n)^2 b_{i+1}^n-(h_i^n)^2 b_i^n}{\Delta x}$$

$$=(S_{bed})_{i+1/2}^n+(S_f)_{i+1/2}^n+(S_{sed})_{i+1/2}^n+(S_c)_{i+1/2}^n+(S_w)_{i+1/2}^n \tag{32}$$

With the discretised source terms given by equation 33 to 37.

$$(S_{bed})_{i+1/2}^n=-\mathrm{g}\hat{h}_{i+1/2}^n b_{i+1/2}^n\left(\frac{z_{i+1}^n-z_i^n}{\Delta x}-\tan(\hat{\theta})_{i+1/2}^n\right) \tag{33}$$

$$(S_f)_{i+1/2}^n=-(u_*^2)_{i+1/2}^n\left[2\cdot(d_{tr})_{i+1/2}^n+b_{i+1/2}^n\right] \tag{34}$$

$$(S_{sed})_{i+1/2}^n=(v_{sed})_{i+1/2}^n\mathrm{u}_{i+1/2}^n\mathrm{b}_{i+1/2}^n\frac{\rho_{settled}-\hat{\rho}_{i+1/2}^n}{\hat{\rho}_{i+1/2}^n} \tag{35}$$

$$(S_c)_{i+1/2}^n=-\frac{1}{2}g(\hat{h}_{i+1/2}^n)^2(c_{i+1}^n-c_i^n)\frac{(\rho_s-\rho_\omega)}{\hat{\rho}_{i+1/2}^n} \tag{36}$$

$$(S_w)_{i+1/2}^n=\frac{1}{2}g(\hat{h}_{i+1/2}^n)^2\frac{b_{i+1}^n-b_i^n}{\Delta x} \tag{37}$$

The evolution of trench width in time and the bed evolution in time is given in discretised version by equation 38 and 39 respectively.

$$\frac{b_i^{n+1}-b_i^n}{\Delta t}=2\cdot v_{wall} \tag{38}$$

$$\frac{z_i^{n+1}-z_i^n}{\Delta t}=(v_{sed})_i^n \tag{39}$$

To prevent the trench width from diverging unbounded, the width evolution is stopped when the trench depth has decreased up to a certain threshold value. This threshold value is set at 0.05m. Furthermore the mixture density at the cell faces is given by equation 40.

$$\hat{\rho}_{i+1/2}^n=\rho_s\hat{c}_{i+1/2}^n+\rho_w(1-\hat{c}_{i+1/2}^n) \tag{40}$$

As stated before, the variables not defined on the grid are denoted with a hat and are determined via an upwind approximation, see equation 41 to 43.

$$\hat{h}_{i+1/2}^n=\begin{cases}h_i^n & if\ u_{i+1/2}^n\geq 0\\ h_{i+1}^n & if\ u_{i+1/2}^n<0\end{cases} \tag{41}$$

$$\hat{c}_{i+1/2}^n=\begin{cases}c_i^n & if\ u_{i+1/2}^n\geq 0\\ c_{i+1}^n & if\ u_{i+1/2}^n<0\end{cases} \tag{42}$$

$$\hat{u}_i^n = \begin{cases} u_{i-1/2}^n & if\ \frac{1}{2}\left(u_{i-1/2}^n + u_{i+1/2}^n\right) \geq 0 \\ c_{i+1/2}^n & if\ \frac{1}{2}\left(u_{i-1/2}^n + u_{i+1/2}^n\right) < 0 \end{cases} \quad (43)$$

The sedimentation velocity v_{sed} entrainment velocity v_E and friction velocity u_* are defined as a function of h, u and c on either the cell centers or faces. The explicit upwind approximations are used when a variable that is not defined on the grid is required.

Treatment Of Moving Boundary Cell

The trencher is moving to the left in a fixed grid, thus being located in different grid cells in time. Due to stability issues, it is not possible for the trencher boundary to move exactly one grid cell every time step. It will take several time steps for the trencher to move one grid cell. As a result, the boundary cell (denoted by subscript b) will grow in size with velocity v_t for the continuity control volumes (eq. 44) and with velocity $v_t/2$ for the momentum control volume. See figure 9, where Δx_b^n is the old boundary cell size and Δx_b^{n+1} The size of the boundary cell in the new time step. The ux going trough the left boundary should therefore be corrected with the growth velocity of the boundary cell.

$$\Delta x_b^{n+1} = \Delta x_b^n + v_t \cdot \Delta t \quad (44)$$

To give the treatment of the boundary cell in a readable expression, the continuity equation for shallow water flow with constant width is used (eq. 45). This is a simplified version of equation 18, with all the source terms included in variable S.

$$\frac{\partial h}{\partial t} + \frac{\partial hu}{\partial x} = S \quad (45)$$

For an explicit treatment of the source terms and the uxes, the discretised expression of equation 45 is now given by equation 46, which can be solved for h_b^{n+1} .

$$\frac{h_b^{n+1}+\Delta x_b^{n+1}-h_b^n \Delta x_b^n}{\Delta t} = S_b^n \cdot \Delta x_b^n - \left[(hu)_{b+1/2}^n - (h(u+v_t))_{b-1/2}^n\right] \quad (46)$$

Empirical Equations For Model Closure

The last unknowns in the set of equations are the active wall velocity v_{wall}, sedimentation velocity v_{sed}, entrainment velocity v_E and friction velocity u_*. The wall velocity for a vertical wall is given by equation 47 (Rhee, 2015), where k_0 is initial permeability, given by equation 48 (Adel, 1987), φ is the internal friction angle, $\Delta = (\rho_s - \rho_w)/\rho_w$, v is kinematic viscosity, n_0 initial porosity and D_{15} 15th percentile grain size.

$$v_{wall} = -10 \cdot k_0 \cdot \Delta \cdot \frac{\sin(\emptyset - \pi/2)}{\sin \emptyset} = -10 \cdot k_0 \cdot \Delta \cdot \cot(\emptyset) \quad (47)$$

$$k_0 = \frac{g}{160 \cdot v} D_{15}^2 \frac{n_0^3}{(1-n_0)^2} \quad (48)$$

The sedimentation velocity is given by equation 49, where S and E are sedimentation and erosion flux respectively and ρ_s is sediment density. For a detailed explanation of the sedimentation and erosion fluxes, see Rhee (2010).

$$v_{sed} = \frac{S-E}{\rho_s \cdot (1-n_s-c)} \quad (49)$$

The entrainment velocity is included via equation 50, where entrainment coeffcient α_E is determined via an empirical function (eq. 51) proposed by Parker et al. (1987). The function convergences to 0.075 for non-stratified ow. The Richardson number is defined as $R_i = g' h/u^2$ with reduced gravity $g' = g(\rho_m - \rho_w)/\rho_w$, where ρ_m is mixture density and ρ_w water density.

$$v_E = \alpha_E \cdot u \quad (50)$$

$$\alpha_E = \frac{0.075}{(1+718 \cdot Ri^{2.4})^{1/2}} \quad (51)$$

The friction velocity is included to account for the friction of the flow at the bed and sidewalls of the trench. The friction velocity is given by equation 52, where f is an empirical factor and u the layer averaged flow velocity. A bed friction factor of f = 0.024 is used, within the range mentioned in (Garcia, 1990).

$$u_* = \sqrt{\frac{f}{8}} \cdot u \tag{52}$$

Boundary And Initial Conditions

On the left (moving) boundary, the flow height, width, concentration and velocity are imposed. In the case of a subcritical flow it is sufficicent to specify only the flow rate instead of both the height, width and velocity. However the volume flux trough the moving boundary is $h \cdot b(u + v_t)$, which cannot be replaced by a flow rate q due to the presence of v_t. Therefore flow velocity u_0 is determined manually as an input, and can be tweaked to make sure the simulation is stable.

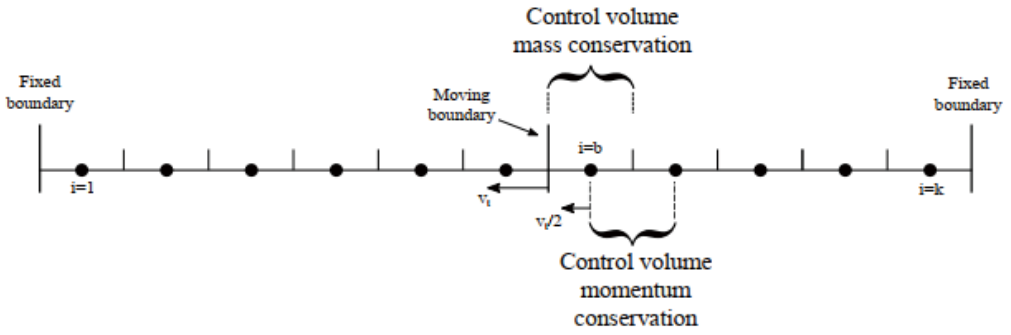

Figure 9. Illustration of spacial grid, indicating the moving and ftxed boundaries. Growth velocity of control volumes for mass and momentum conservation are indicated by v_t and $v_t/2$ respectively.

The right boundary is an outflow boundary, where a zero-gradient boundary condition is imposed. For this assumption to be valid, fluctuations should be minimal towards the right boundary. The initial conditions are therefore chosen such that the bed elevation and trench width are constant close to the right boundary. To achieve this, the initial location of the moving boundary is set at a certain distance (default 5m) from the right boundary. The bed elevation is set at zero and the flow velocity, height and width are set equal to the output values of the erosion model. The bed elevation and trench width are then constraint such that they will remain constant in this section.

Stability Of The Scheme

For the scheme to be stable it has to satisfy the Courant-Friedrichs-Lewy (CFL) condition, given by equation Where CFL is the dimensionless CFL number, u_{max} is the maximum velocity in the domain, Δt the time step and Δx_{min} the smallest possible grid grid size in the domain.

$$\text{CFL} = \frac{|u_{max}| \cdot \Delta t}{\Delta x_{min}} \leq 1. \tag{53}$$

The trencher boundary moves to the left in the grid in time, dependent on trencher velocity and time step. In one time step, the boundary cell will grow by a distance equal to Δx_{min}, which is also the smallest grid size occurring in time. The CFL condition for this cell is given by equation 54. From this relation it can be concluded that the CFL condition for the boundary cell can only be fulfilled if the trencher velocity is greater or equal to the flow velocity ($v_t \geq |u_{max}|$). In other words, the stability of the scheme, with regard to the CFL condition for the boundary cell, is independent of the time step. However, since a quite robust scheme (explicit, upwind) is used, the CFL number can be higher than one. Also, since there only is one grid cell that does not fulfill the CFL condition, the error created dampens out in the rest of the domain.

$$\text{CFL} = \frac{|u_{max}| \cdot \Delta t}{v_t \cdot \Delta t} = \frac{|u_{max}|}{v_t} \tag{54}$$

Veriftcation

This section aims to verify whether the proposed numerical scheme is able to capture the phenomena that can occur in shallow water flows. Examples of these phenomena are propagating shocks and transitions between subcritical and supercritical flows and vice versa (hydraulic jumps). To do this verification, the numerical scheme is applied on several scenarios for which exact analytical solutions are known. Analytical solutions are taken from the SWASHES library (Delestre et al., 2016), in which numerous analytical solutions for the shallow water equations are summarised. Four different cases are used for this verification; a dam-break, subcritical flow

over a bump and transcritical flow over a bump with and without a hydraulic jump. Results are given in figures 10 to 13.

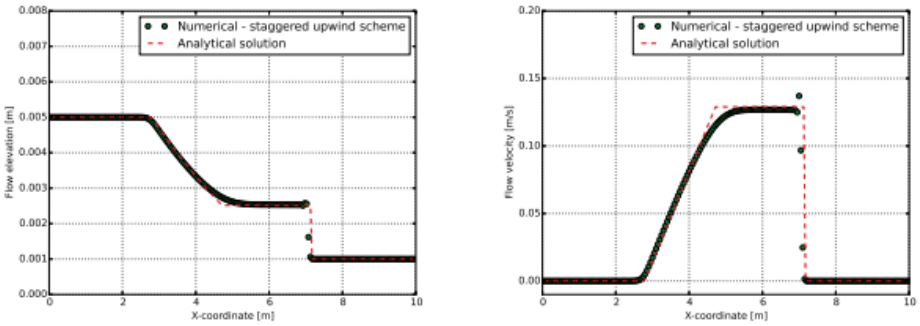

Figure 10. Comparison of the dam-break analytical and numerical solution for the staggered upwind scheme. Shown is flow elevation (a) and velocity (b), snapshot at T = 9sec.

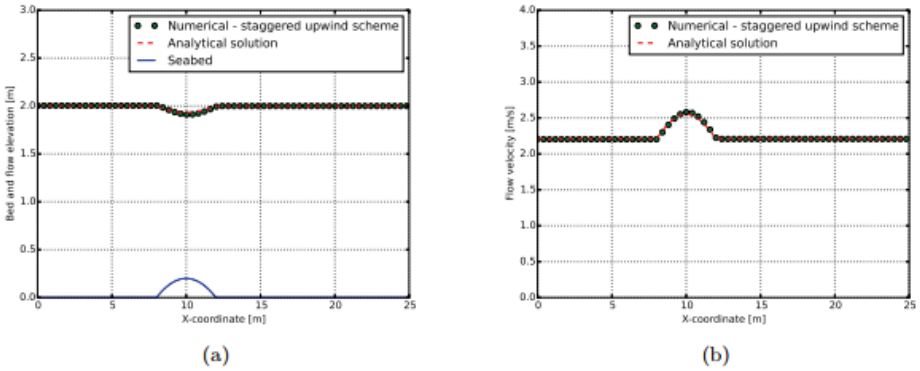

Figure 11. Comparison of analytical and numerical solution of the staggered upwind scheme for a subcritical flow over a bump. Shown is flow elevation (a) and velocity (b).

Results of the verification show that the scheme is shock-capturing and performs reasonably well. Some deviation in the discharge is observed at the hydraulic jump location in figure 13. However this is not an issue within the current application of the scheme, since an overall trench profile is the objective and not accurate local values of the discharge.

CABLE DEFLECTION MODEL

The burial depth of the cable is determined by the intersection of the cable shape and the re-settled seabed. The cable shape is based on an elastic, hyperstatic cantilever beam model which is uniformly loaded. The left hand side is completely fixed and the right hand side is restrained in rotation. The residual lay tension in the cable is applied at the right hand side of the cantilever beam. It is assumed that the position of the

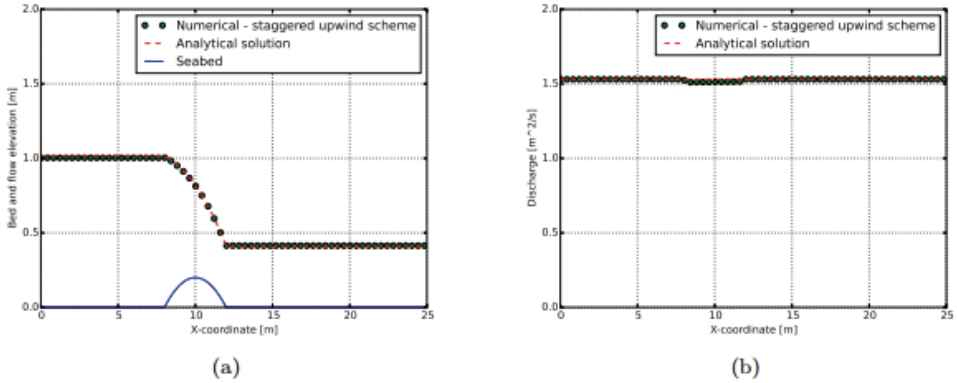

Figure 12. Comparison of analytical and numerical solution of the staggered upwind scheme for a transcritical flow over a bump, without hydraulic jump. Shown is flow elevation (a) and discharge (b).

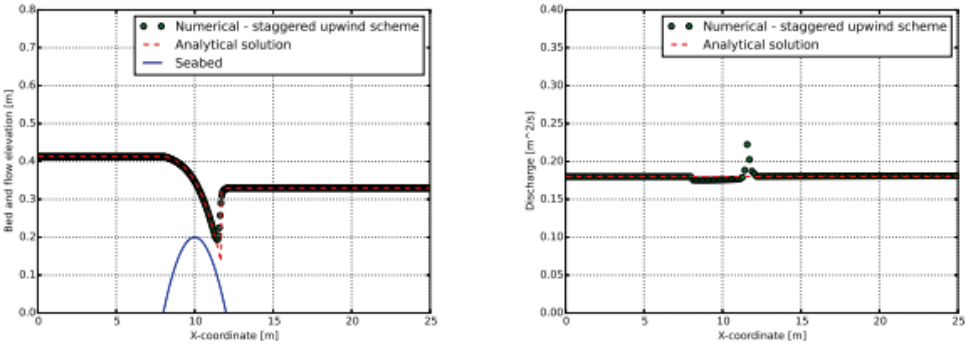

(a) (b)

Figure 13. Comparison of analytical and numerical solution of the staggered upwind scheme for a transcritical flow over a bump, with hydraulic jump. Shown is flow elevation (a) and discharge (b).

cable remains fixed when the touchdown point intersects with the trench shape. The analytical solution for the cantilever beam is given in Vanden Berghe et al. (2011). Exact assumptions in the derivation of the equation are unknown, therefore a verification has been done by comparing the analytical solution to numerical solutions generated by OrcaFlex, which is a dynamic analysis package used within the offshore industry.

$$z(x) = -\left[\frac{qL}{T}\cdot\sqrt{\frac{EI}{T}}\cdot\frac{\cos h\left(\sqrt{\frac{T}{EI}}L\right)}{\sin h\left(\sqrt{\frac{T}{EI}}L\right)}\cdot\right.$$

$$\left.\left[\cos h\left(\sqrt{\frac{T}{EI}}x\right) - tanh\left(\sqrt{\frac{T}{EI}}x\right)\cdot sinh\left(\sqrt{\frac{T}{EI}}L\right) - 1\right] - \frac{q}{2T}x^2 + \frac{qL}{T}x\right] \quad (55)$$

Where z is the cable deflection measured from the seabed, q is cable weight , T is residual lay tension, L is distance until touchdown point, EI is bending stiffness and x is the distance from start of the trench. The cable deflection equation is incorporated in the sedimentation model and is solved each time a new grid cell is created at the moving boundary. The cable is not lowered in clear water but in a mixture of sediment and water, the cable weight should thus be corrected. A single reference concentration is chosen to correct the cable weight. This reference concentration is chosen to be equal to the concentration at the interface of erosion and sedimentation model.

$$q_{slurry} = q_{water} + c_{ref}\cdot D^2\cdot\frac{\pi}{4}\cdot(\rho_w - \rho_s)\cdot g \quad (56)$$

Where q_{slurry} is the cable weight in the water sediment mixture, qwater is the cable weight submerged in water, c_{ref} the reference concentration of sediment, D is cable diameter, ρ_w and ρ_s are water and sediment density respectively.

RESULTS

A typical output of the model is given in figure 14, showing a side view, top view and the concentration development behind the trencher.

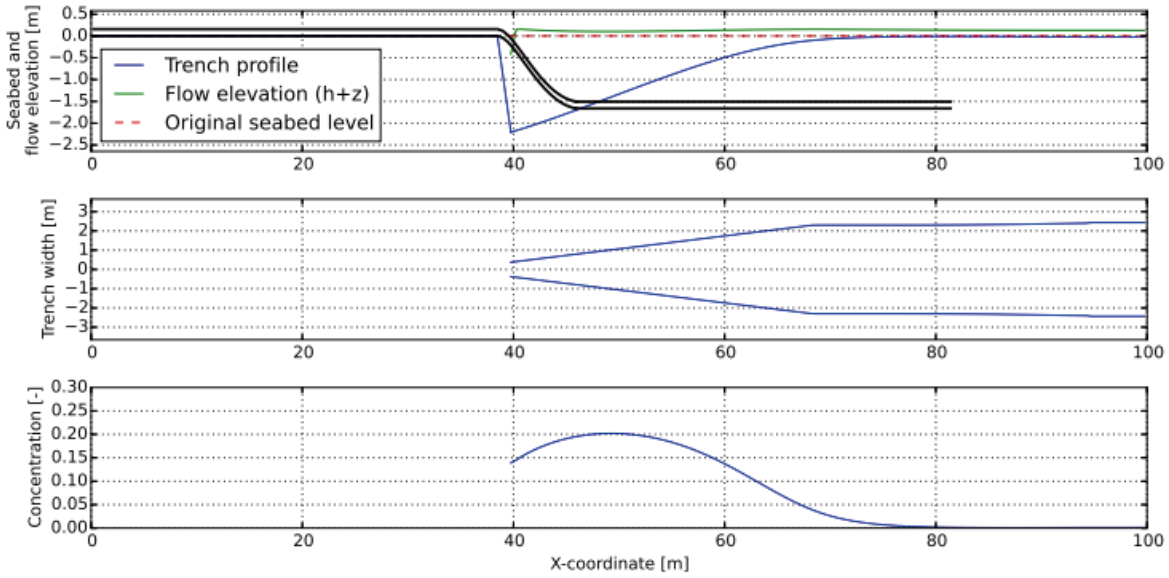

Figure 14. Model results for $D_{15} = 0.15mm$, $D_{50} = 0.3mm$ and $v_t = 0.1m/s$. Top plot shows a side view of the trench, second plot shows a top view of the trench with the development of trench width, the lowest plot shows the depth averaged sediment concentration.

Model Validation

To validate the jet trenching model, averages of the depth of lowering are taken per cable section (monopile to monopile). To account for uncertainties in grain size and residual cable tension, a minimum and maximum depth of lowering case is considered. The minimum case is based on ($d_{15} = 0.2mm$, $d_{50} = 0.4mm$, $T = 5kN$) and the maximum case on ($d_{15} = 0.1mm$, $d_{50} = 0.25mm$, $T = 2kN$). Per individual cable section the average jet pressure and trencher velocity is extracted from logs recorded during trenching. Furthermore the sword depth and nozzle configuration are known per cable section. As a result a minimum and maximum depth of lowering is calculated per cable section, indicated by the red and blue lines in figure 15. The results show that approximately 83% of the cable sections are within the predicted range.

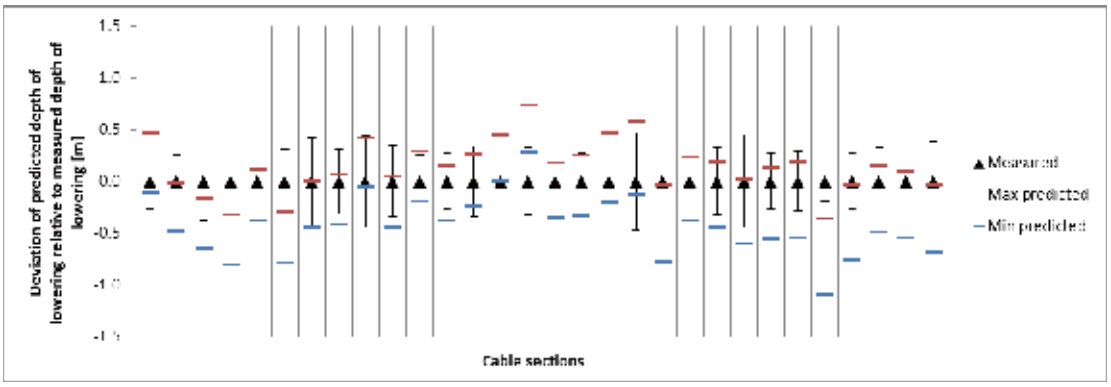

Figure 15. Validation of the jet trenching model by comparing predicted range to measured results during a reference project. Error bars indicate standard deviation in measured depth of lowering.

Although the average depth of lowering is hardly influenced by sand dunes in the model, the local depth of lowering can be higher or lower due to the presence of sand dunes. To validate whether this effect is correctly included in the model, the depth of lowering for a cable section is compared to that measured during a reference project. The selected section of seabed profile has a sand dune height and length of approximately 0.5m and 12.5m respectively (figure 16). The seabed profile is somewhat smoothened by applying a moving average before importing it into the model. In figure 16 the smoothened seabed profile is plotted together with the measured and predicted cable position. The cable position predicted by the model follows a pattern in phase with the sand waves, whereas the measured cable position shows an out of phase pattern with the sand dunes.

However, not the absolute cable position but the cable position relative to the seabed (depth of lowering) is important. The measured and predicted depth of lowering are plotted in figure 17. Difference between minimum and maximum depth of lowering measured is approximately 0.8m, whereas the predicted difference is approximately 0.2m, this is thus a significant underestimation.

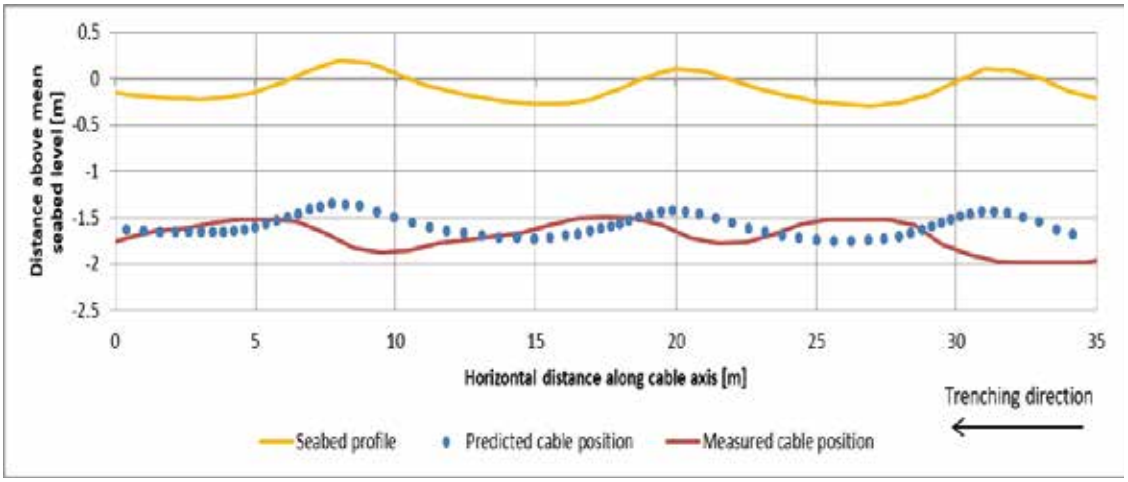

Figure 16. Seabed proftle used as model input and measured/predicted cable position.

Model Results

The effect of having a higher trencher velocity depends on grain sizes. In coarse sand the increase in depth of lowering is larger than in fine sand for the same increase in trencher velocity, see figure 18. Therefore it is more important to have a high trencher velocity in coarse sand than in fine sand.

Sand dunes, characterised by their height and length, are modelled as a simple sinusoidal profile. Due to the seabed profile, also the depth of lowering shows an oscillating profile. To indicate this behaviour, the bandwidth (minimum and maximum values) and mean depth of lowering is plotted. To investigate sensitivity of sand dune length, the height is kept constant and only dune length is varied, see figure 19. The bandwidth shows a clear local minimum at a wavelength of approximately 7.5m. This is an interesting wavelength since

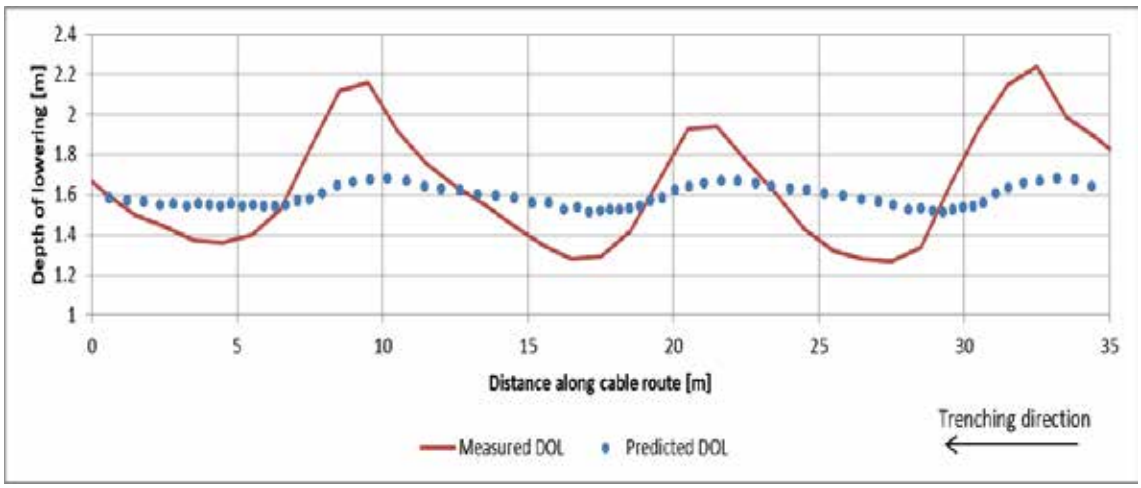

Figure 17. Measured and predicted depth of lowering.

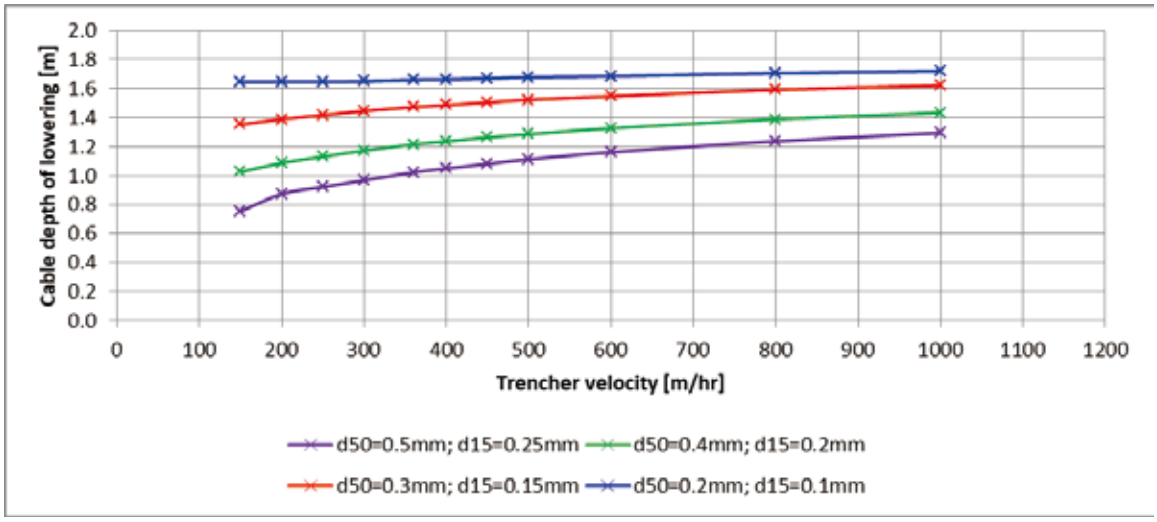

Figure 18. Cable depth of lowering for a range of trencher velocities and four different d_{50}.

it is approximately equal to the layback of the cable (distance from start of trench to touchdown point of cable). For a wavelength of half the layback and 1.5 times the layback, there is a maximum in the bandwidth. Thus when the start of the trench is in phase with the touchdown point of the cable the variation of depth of lowering is minimum. However, the mean depth of lowering is hardly influenced.

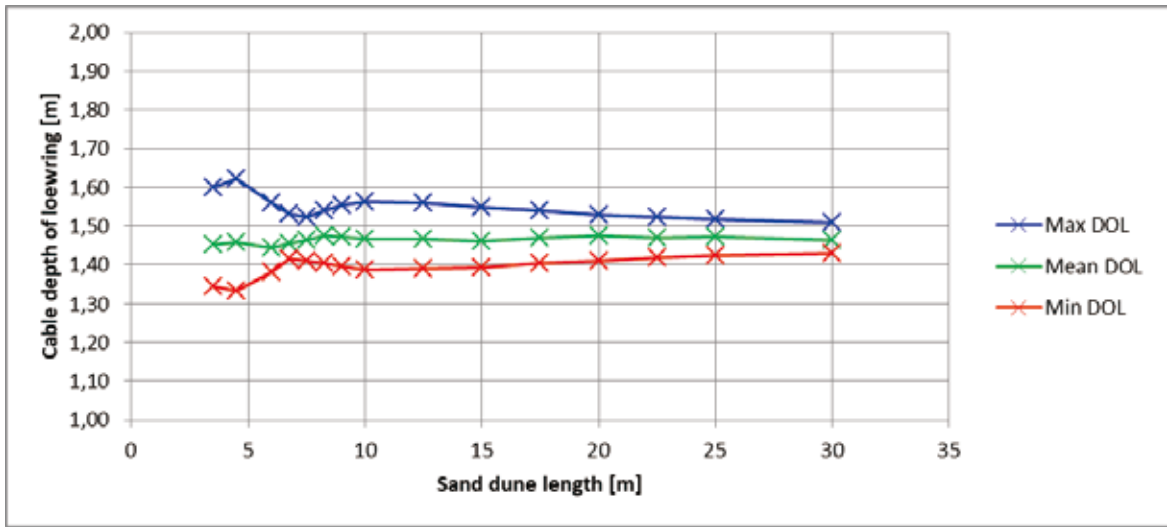

Figure 19. Cable depth of lowering for a range of sand dune lengths, and constant sand dune height of 0.4m.

A similar plot but now for sand dune height is given in figure 20. The bandwidth shows to increase almost linearly with sand dune height, and again the mean depth of lowering is hardly influenced by sand dune height.

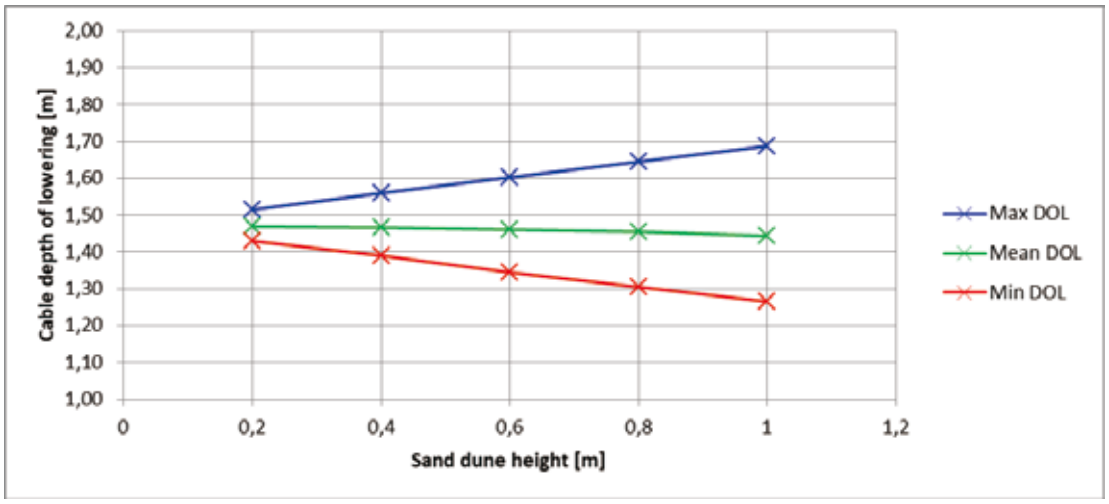

Figure 20. Cable depth of lowering for a range of sand dune heights, and constant sand dune length of 12.5m.

Discussion

The amplitude at which the depth of lowering oscillates when buried in sand dunes, is shown to be underestimated by the model compared to field data. An explanation could be the relatively simple cable equation used in the model. This equation takes the tension as a constant and uses this to calculate the cable shape. However it is expected that while the cable is being lowered in the trench on sand dunes, the tension in the cable varies. This might have a significant influence on the depth of lowering, but requires further investigation.

Although the current model is able to cope with hydraulic jumps, it is not possible to include a supercritical inflow at the moving boundary. The high flow velocity required for this supercritical inflow results in instabilities initiated at the boundary cell. The inflow is therefore taken to be subcritical with a large flow height and low flow velocity. By applying a cell merging technique on the boundary cell, the stability can be increased, allowing for a supercritical inflow.

CONCLUSIONS

A jet trenching model is proposed, which includes breaching, erosion, sedimentation and entrainment to make an accurate prediction of the depth of lowering of a cable buried in sand. By verification against analytical solutions of the shallow water equations, the numerical scheme of the sedimentation model shows to be shock-capturing and performing accurately. When considering cable burial in sand dunes, an oscillating depth of lowering trend is observed, with the maximum depth of lowering at sand dune crests and minimum at the troughs. This pattern is resulting both from field measurements and model simulations. However, the amplitude in depth of lowering variation is significantly underestimated by the model. Validation shows that the depth of lowering of approximately 83% of the cable sections of a reference project is within the range predicted by the model. By investigating the effect of grain sizes and trencher velocity, it has been shown by the model that it is more important have a high trencher velocity in coarse sand than in fine sand.

REFERENCES

Adel, H. den (1987). “Heranalyse doorlatendheidsmetingen door middel van de forch-heimer relatie (in dutch)”.

Cao, C., Pender, G., Wallis, S., and Carling, P. (2004). “Computational Dam-Break Hydraulics over Erodible Sediment Bed”. *Journal of Hydraulic Engineering* 130(7), 689–703.

Delestre, O., Lucas, C., Ksinant, P. A., Darboux, F., Laguerre, C., Vo, T., James, F., and Cordier, S. (2016). “SWASHES: a compilation of shallow water analytic solutions for hydraulic and environmental studies”. International Journal for Numerical Methods in Fluids 72(3), 269–300.

Garcia, M. (1990). “Depositing and eroding sediment-driven flows: Turbidity currents”. University of Minnesota.

He, S., Liu, W., Li, X., and Ouyang, C. (2014). “An improved coupling model for water flow, sediment transport

and bed evolution". *Journal of Geoscientific Model Development* 7, 2429–2454.

Jong, P. de (1988). "Een productie optimalisatie van het gebruik van spuiters op de sleephopperzuiger Volvox Delta". MA thesis. Technische Universiteit Delft.

Lee, J. and Chu, V. (2003). *Turbulent jets and plumes: A lagrangian approach*. Kluwer Academic Publishers. Miedema, S. (2015). OE4607 *Introduction to Dredging Engineering*. 2nd ed. Delft University of Technology.

Nobel, A. (2013). "On the excavation process of a moving vertical jet in cohesive soil". PhD thesis. Delft University of Technology.

Parker, G., Garcia, M., Fukushima, Y., and Yu, W. (1987). "Experiments on turbidity currents over an erodible bed". *Journal of Hydraulic Research* 25(1), 123–147.

Rhee, C. van (2010). "Sediment Entrainment at High Flow Velocity". *Journal of Hydraulic Engineering*

136(9), 572–582.

Rhee, C. van (2015). "Slope failure by unstable breaching". *Proceedings of the ICE - Maritime Engineering*

168, 84–92.

Robert, S. and Wilson, P. (2011). "A well balanced scheme for the shallow water wave equations in open channels with (discontinuous) varying width and bed". *Austral. Mathematical Soc.* 52, 967–987.

Saint Venant, A. (1871). "Theorie du mouvement non-permanent des eaux, avec application aux crues des rivieres et a l'introduction des marees dans leur lit". *Comptes Rendus de l'Academie des Sciences* 73, 147–154.

Siviglia, A., Nobile, G., and Colombini, M. (2008). "Quasi-Conservative Formulation of the One-Dimensional Saint-Venant–Exner Model". *J. Hydraul. Eng.* 134(10), 1521–1526.

Vanden Berghe, J., Pyrah, J., Gooding, S., and Capart, H. (2011). "Development of a jet trenching model in sand". *Frontiers in Offshore Geotechnics* 2, 889–894.